Increased Displacement in Magnetomotive Ultrasound Imaging by Adding a Homogeneous Magnetic Field

Jules Reniaud

2022

LUND
UNIVERSITY

Master's Thesis in Biomedical Engineering

Faculty of Engineering LTH
Department of Biomedical Engineering

Supervisor: Tomas Jansson
Examiner: Magnus Cinthio

Abstract

Magnetomotive Ultrasound, MMUS, is an imaging modality used to reveal a magnetic contrast agent using an external time-varying inhomogeneous magnetic field. By this, the particles are set in motion, and the motion is detected with ultrasound. The technique has applications in cancer detection but is limited in penetration as the magnetic field decreases rapidly with distance. Instead of increasing the size of the conventionally used magnetic probe which would lead to heating and clinical practicality problems, adding a homogeneous magnetic field has been suggested to increase the force and thereby displacement. Since the magnetic force is proportional to both the magnetic field strength and the field gradient, the second homogeneous field will increase the force. The force is also proportional to the magnetic susceptibility of the contrast agent which is increased by this second field (pre-magnetization). A homogenous magnetic field was generated using a Helmholtz coil (2x150 turns) driven by an AC current (5 Hz, 4 A peak to peak) synchronized in phase with the rotating neodymium magnet generating the inhomogeneous field (also 5 Hz). The fields set in motion magnetic particles embedded in a tissue-mimicking material and the tissue motion was imaged using an ultrasound scanner (Visualsonics F2). The images were processed using the previously published algorithm to measure the axial component of the tissue motion. The homogeneous field reached a peak value of 6 mT at the center of the coil, this in addition to the magnetic field produced by the rotating neodymium magnet. The displacement in each image pixel, averaged over a region of interest encompassing the nanoparticle insert, versus distance from the face of the rotating magnet is greater when the coil is added. Similarly, the displacement increases as a function of the homogeneous magnetic field in both directions of the circular motion. Adding the coil with a homogeneous field does increase the detected magneto-motion, in accordance with the theoretical model. This points to a possible way to increase the sensitivity in MMUS by adding a homogeneous magnetic field.

Populärvetenskaplig sammanfattning

Medicinska bilder spelar en stor roll för att ställa diagnoser och styra terapi. Olika discipliner som radiologi, endoskopi eller mikroskopi används för att skapa bilder på människan, alla med olika syften. Diagnostiskt ultraljud är en av dessa bildgivande metoder. En så kallad prob sänder ut ljud i olika riktningar och med ledning av de mottagna ekona kan en bild byggas upp av kroppens inre. Jämfört med andra tekniker är ultraljud icke-invasiv, billig, ger realtidsbilder och avger inte joniserad strålning. Metoden är en av de vanligaste inom dagens sjukvård men har fortfarande sina begränsningar och utmaningar.

En ny metod som är under utveckling kallas magnetomotoriskt ultraljud, eller MMUS efter engelskans magnetomotive ultrasound. Magnetiska nanopartiklar injiceras i kroppen och kan tas upp av specifik vävnad. Dock är partiklarna för små för att synas i ultraljudsbilder. För att komma runt det kan partiklarna sättas i rörelse med hjälp av ett varierande magnetfält. De sätter då också sin närmaste omgivning i rörelse, och den rörelsen kan detekteras med ultraljud. MMUS gör det möjligt att skapa en helt ny typ av bilder som baseras på molekylära processer snarare än anatomiska förändringar. Detta eftersom man kan märka nanopartiklarna så att de fastnar på olika signalmolekyler som är karakteristiska för en typ av sjukdom. Molekylär avbildning, som angreppssättet kallas, har tidigare bara gjorts med ett begränsat antal tekniker, såsom exempelvis Positronemissionstomografi (PET).

Denna utveckling av medicinskt ultraljud erbjuder nya användningar som till exempel för kolorektalcancer. Kolorektalcancer är den tredje vanligaste cancerformen i världen och den andra orsaken till cancerrelaterad död. Behandlingen innefattar en kombination av kirurgi, strålbehandling, kemoterapi och riktad behandling. Dock dör många patienter även efter behandlingen eftersom cancern har spridit sig utan att det kunnat upptäckas. Därför blir det kritiskt att veta om cancer har redan spridit sig vilket sker med metastaser till intilliggande lymfnoder. Tanken är att injicera nanopartiklar nära tumören, varvid partiklarna följer samma väg i lymfbanorna som tumörcellerna. Sedan kan man med MMUS se nanopartiklarnas upptag i lymfnoder, och därigenom bättre bedöma patientens risk för tumörspridning.

En av begränsningarna med MMUS idag är undersökningsdjupet. I fallet

med kolorektalcancer används en roterande permanentmagnet, vilket fungerar väl för den tillämningen. Dock avtar fältstyrkan avtar relativt snabbt med avståndet. För att kunna använda tekningen för andra tillämpningar hade det varit värdefullt att kunna utöka mätdjupet.

Under mitt exjobb har jag undersökt hur rörelse av partiklar påverkas när de finner sig i ytterligare ett homogent magnetfält. Först visade jag med en teoretisk modell att ett homogent magnetfält ökar kraften som verkar på partiklarna och att ökningen sker i båda rörelseriktningarna. Sedan byggde jag en Helmholtzspole, som är en vanlig lösning som används för att alstra ett i princip homogent magnetfält, och mätte rörelsen av partiklar i en fantom med MMUS-tekniken. Jag observerade att rörelsen var större med det extra magnetfältet i både rörelseriktningarna enligt vad teorin förutspått. Med den ökade rörelsen förbättras detektionsförmågan hos MMUS vilket kan vara en lösning för andra tillämpningar som exempelvis kolorektalcancer.

Acknowledgements

First of all, I would like to thank my supervisor Tomas Jansson for giving me the opportunity to work on the project. It has been a pleasure working with you and I learned a lot thanks to your precious help and advice. Thank you to the ultrasound group for all the information you provided me with and for the group meetings which were always very interesting. Thank you Magnus Cinthio for being my examiner, Sandra Sjöstrand for the practical help with the magnetomotive set-up. Tobias Erlöv, thank you for the hand you gave me when processing the data with Matlab.

A big thank you to all the members at the Department of Biomedical Engineering, Axel Tojo for helping me building the coil, Désirée Jarebrant for the useful information, and all the other persons I had the pleasure of talking to. Thanks to you, I had a great time working on my project at the department.

Thibaut Valéry, I can not thank you enough for your friendship, for all the discussions around my project and for always being there. This goes also for Linda Péroux, Damien Gauthier and Fred Celle with whom I spent so many wonderful moments.

Lastly, I would like to thank my family and friends for supporting me all along the project and throughout my stay in Sweden.

Contents

1 Introduction

1.1 Background

1.1.1 Magnetomotive ultrasound

Ultrasound imaging is a widely used imaging technique using high-frequency sound waves to view inside the body. Having the advantages of allowing for real time imaging, being widely available, inexpensive and free from ionising radiation, the technique is a competitive alternative to other standard imaging modalities such as Magnetic Resonance Imaging (MRI), Positron Emission Tomography (PET) or even X-rays.

Ultrasound imaging is used to create an image of internal body structures using the sound echoes coming back when reflected on the structures. It is famously used for observing fetal growth. The technique was improved using contrast agent to become contrast-enhanced ultrasound (CEUS). Contrast agent are gas filled micro-sized bubbles reflecting highly the ultrasound echoes thus increasing the contrast with surrounding tissues. In addition to enhancing the contrast, the micro-bubbles can be used for therapeutic applications. The micro-bubbles can be loaded with a specific drug through different processes. Once the bubble has reached the targeted area, its membrane is rendered permeable with ultrasound, thus releasing the drug (Mulvana et al. 2017). In other applications, micro-bubble contrast agent is used to open physiological barrier such as the blood brain barrier (BBB). Ultrasound-induced BBB opening has been shown to increase the penetration of chemotherapeutic agents in the brain leading to new ways to improve brain cancer treatments (Dréan et al. 2019).

However, one limitation of micro-bubbles is their size which confines them to the vascular system (Barua et al. 2014) when other imaging modalities have the ability to image cellular and molecular processes for what is called molecular imaging. Rather than observing the induced anatomical changes, molecular imaging shows the molecular basis of a disease. PET or Optical Coherence Tomography (OCT) for example, are available molecular imaging techniques (Avril et al. 2001), (Tian 2013). Using smaller contrast agent particles in ultrasound imaging has proven to be a problem since the scattering cross section of a particle decreases with the sixth power of the radius of the particle (Cobbold 2006). To get past this problem, using a

magnetic contrast agent was considered. Using an external magnetic field, the contrast agent is set in motion and the motion is detected with ultrasound to get information on the presence and location of the agent. This idea was first applied with Magnetomotive Optical Coherence Tomography (MMOCT) where the motion is tracked with low-coherence light. Magnetomotive ultrasound (MMUS) uses the same principle as MMOCT but uses ultrasound to track the movement instead of light.

The movement measured using ultrasound is in fact not the motion of the contrast agent itself but of the surrounding tissues. The motion of the tissue depends on the tissue mechanical properties which can be affected by disease progression. Assessing the mechanical properties of a tissue with MMUS can thus give important information for diagnostics (Sjöstrand 2021) and is thus one of the possible applications.

1.1.2 Operating principle

Magnetomotive ultrasound uses a magnetic contrast agent which is set in motion thanks to an external time-varying magnetic field. The time-varying motion of tissue surrounding the embedded magnetic contrast agent is imaged using an ultrasound scanner.

Creating a strong enough magnetic field is essential to induce a detectable motion of the magnetic particles. Experiments report using a solenoid with an iron core to produce a time and space varying magnetic field (Sjöstrand 2021). The electromagnet can be placed on the opposite side or on the same side of the object as the ultrasound probe (figure 1). However, solenoids require large currents to achieve a strong magnetic field and are therefore prone to heating. In addition, solenoids appeared not very suitable for clinical application as they are large devices. Permanent magnets, as they are smaller in size and less prone to heating were found to be more suitable for clinical use. Permanent magnets generate static magnetic field which can be made time-varying by rotating the magnet around an axis orthogonal to the magnetization. The magnetic field intensity at a given point will oscillate at a given frequency related to the rotation frequency of the motor. Studies showed that such a way to generate the magnetic field was similar to using a solenoid with an iron-core in terms of magnitude of the magnetic field intensity (Sjöstrand et al. 2018).

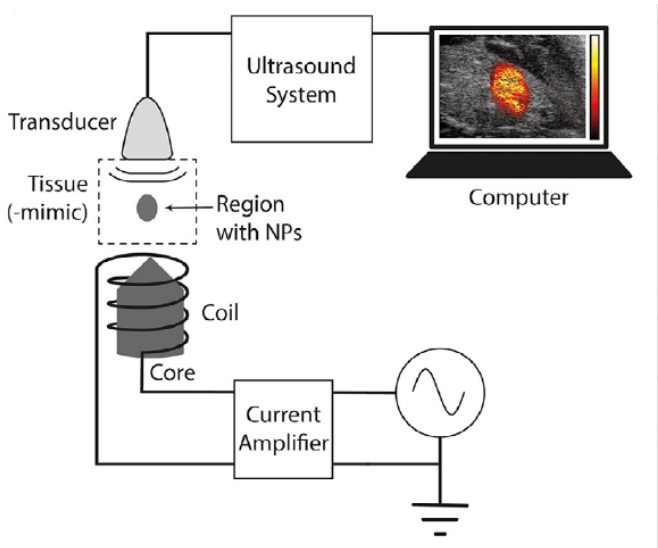

Figure 1: Schematic overview of a magnetomotive ultrasound (MMUS) imaging system. Nanoparticles (NPs) are present in a tissue and set in motion using coil with an iron core. The displacement of the NPs is measured with an ultrasound system. (Sjöstrand et al. 2020).

In addition to the magnetic field, the magnetic particles are also a critical aspect of magnetomotive ultrasound as they need to move in response of the field as well as be safe for the patient. They also need to be able to reach the targeted area.

The most commonly used magnetic contrast agent is superparamagnetic iron oxide nano-particles (SPION). SPIONs have the advantage of begin already used as a MRI contrast agent and are already approved (Bao et al. 2013). The size of commercial SPIONs ranges from 60nm to 150nm and are thus small enough to reach extravascular space. Using a special coating on the nano-particles allows for targetable delivery with localization in a specific area. The coating has to be non toxic and bio-compatible. With the right coating, magnetic particles can bind to drugs, proteins, enzymes or antibodies and can be directed to an organ, tissue or tumour (Gupta et al. 2005).

1.1.3 Magnetomotive force

To evaluate the force acting on the magnetic particles in a magnetic field, let us first consider the magnetic energy U:

$$U = -\overrightarrow{m} \cdot \overrightarrow{B} \tag{1}$$

where B is the magnetic field and m the magnetic moment. The magnetic field B is written:

$$\overrightarrow{B} = \mu_0(\overrightarrow{H} + \overrightarrow{M}) \tag{2}$$

with μ_0 the magnetic permeability, H the magnetic field strength and M the magnetic moment per unit volume. M relates to the magnetic moment m:

$$\overrightarrow{m} = \rho V \overrightarrow{M} \tag{3}$$

The magnetic moment per unit volume M is in reality not linearly proportional to the magnetic field strength H. This non linear relationship is described by the Langevin function (J. H. Oh 2006):

$$M(H) = NmL(\frac{\mu_0 mH}{kT}) \tag{4}$$

with L the Langevin function ($L(x) = coth(x) - \frac{1}{x}$), N the number of atoms per unit volume, m the magnetic moment per atom, k Boltzmann's constant and T the temperature. However, in a weak magnetic field, M depends approximately linearly on the magnetic field intensity H and can be thus written:

$$\overrightarrow{M} = \overrightarrow{M_0} + \frac{\chi}{\rho}\overrightarrow{H} \tag{5}$$

where M_0 is the initial magnetization, *i.e.* the magnetization of the particles in the absence of the applied magnetic field. M_0 depends on the prior history of magnetization of the particles. χ is the magnetic susceptibility and describes formally the slope in the linear region of the Langevin curve (figure

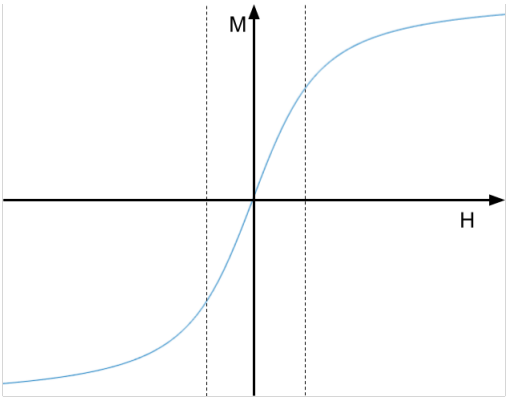

Figure 2: Magnetic moment as a function of the magnetic field intensity (Langevin function). For a weak magnetic field, the relationship can be approximated as linear.

2). Physically, it describes to what extent the particles will be magnetized in a magnetic field.

M can be expressed as a function of the magnetic field B, resulting in an expression of the magnetic moment m:

$$\overrightarrow{M} = \overrightarrow{M_0} + \frac{\chi}{\rho\mu_0}\overrightarrow{B} \tag{6}$$

$$\overrightarrow{m} = \rho V(\overrightarrow{M_0} + \frac{\chi}{\rho\mu_0}\overrightarrow{B}) \tag{7}$$

From the magnetic energy (equation (1)), the magnetomotive force is derived (Shevkoplyas et al. 2007):

$$\begin{aligned} \overrightarrow{F_m} &= -\nabla U \\ &= \nabla(\overrightarrow{m} \cdot \overrightarrow{B}) \\ &= (\overrightarrow{m} \cdot \nabla)\overrightarrow{B} \end{aligned} \tag{8}$$

and thus, substituting m in equation (8):

$$\overrightarrow{F_m} = \rho V(\overrightarrow{M_0} \cdot \nabla)\overrightarrow{B} + \frac{\chi V}{\mu_0}(\overrightarrow{B} \cdot \nabla)\overrightarrow{B} \tag{9}$$

1.1.4 Colorectal cancer

Colorectal cancer is the second leading cause of cancer related death (Pisani et al. 1999). The treatment consists of surgical resection of the colon completed with adjuvant therapy. However, even whith detection and treatment, a large amount of patients succumbs to metastasis cancer. Assessing the spread of cancer within the body has become essential.

The lymphatic system is a circulating system which helps maintain fluid balance in the body. The lymphatic system is punctuated by small masses of lymph tissue called lymph nodes. When a cancer tumor is evolving, cancerous cell can leave the first tumor to migrate and settle in other organs. Those cancerous cells are called metastases. When spreading, they are collected by the lymphatic system and accumulate in the lymph node closest to the tumor. Therefore, a common technique is to retrieve the patient lymph nodes to assess the spread of the tumor (Mulsow et al. 2003).

In an ambition to reduce invasive surgery for the patients, MMUS was considered to evaluate the progression of metastases in lymph nodes. Magnetic contrast agent is injected in the tumor and will migrate along the same path as metastasis proliferation. As uptake of contrast agent is different in healthy and diseased tissue, its presence can be used to map out metastasis progression. The medical examination can be easily performed by the patient's bed.

1.2 Aim

Magnetomotive ultrasound relies on the motion of the magnetic contrast agent injected to the patient as the displacement it induces to the surrounding tissues is what generates the information. Increasing the displacement is a key to a better detection ability in magnetomotive ultrasound and its applications. The displacement is caused by the external field acting on the particles through the magnetomotive force whose expression was derived previously (equation (9)). The force depends mainly on the contrast agent characteristics and on the magnetic field.

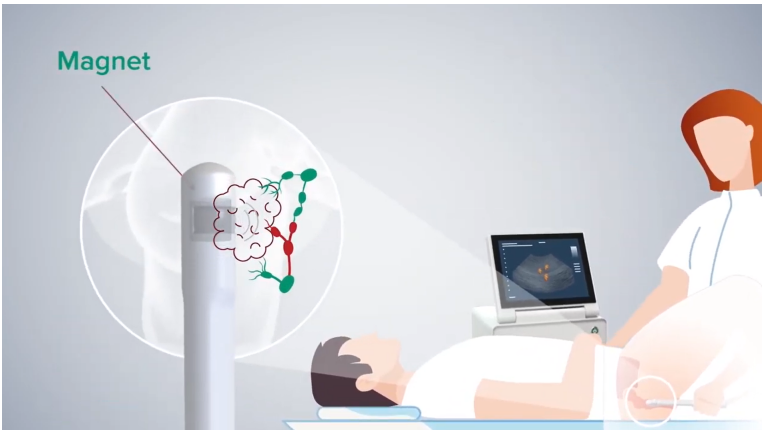

Figure 3: Magnetomotive ultrasound for colorectal cancer. The probe contains a rotating magnet and an ultrasound probe to detect nanoparticles in the lymph nodes. (*NanoEcho* 2022).

For this reason, generating the magnetic field is a critical point in magnetomotive ultrasound. Clinical applications requires strong magnetic fields created by magnets with reasonable sizes and that are safe for the patient. It was shown that using a neodymium magnet could solve some of the issues regarding dimensions and heating (Sjöstrand et al. 2018). However, the magnetic field from the permanent magnet decreases rapidly with distance and is only similar to the field generated by a solenoid at close range (Sjöstrand et al. 2018), limiting the potential applications.

New strategies have been investigated to increase the magnetomotive force acting on the particles through new ways of applying the magnetic field. (Wang et al. 2019) suggests the use of a permanent magnet to magnetize the magnetic particles prior to applying the time-varying magnetic field, providing higher magnetization of the contrast agent and thus a higher force and greater displacement. In the experiment, the electromagnet is on the same side as the ultrasound probe and a static magnet is added close to the particles (figure 4). This additional field increased the measured displacement (figure 5).

The idea of having an additional magnetic field is promising and needs to be pursued. Following the idea of immersing the particles in a magnetic field while performing magnetomotive ultrasound with an other field, the

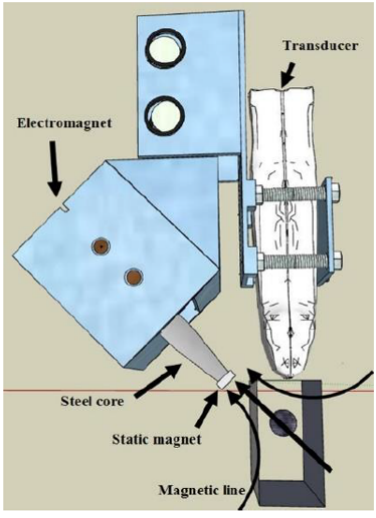

Figure 4: Setup of MMUS with permanent magnet for premagnetization of magnetic contrast agent (Wang et al. 2019).

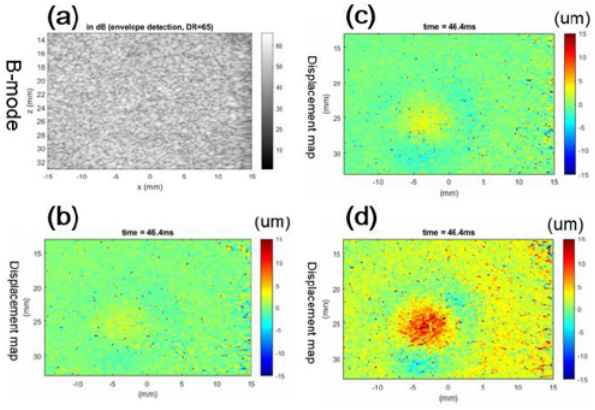

Figure 5: (a) B-mode image for the phantom with embedded magnetic particles. (b) Displacement map without permanent magnet. (c) and (d) Displacement map with permanent magnet (different types) (Wang et al. 2019).

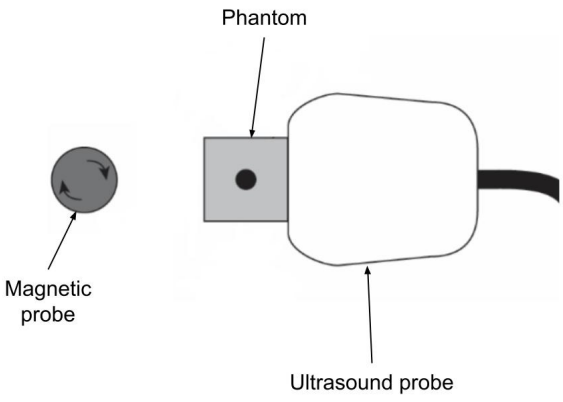

Figure 6: Current technique of magnetomotive ultrasound. The magnetic probe is composed of a permanent magnet diametrically magnetised rotating around an axis orthogonal to the magnetization.

idea of using a Helmholtz coil instead of a permanent magnet emerged. A Helmholtz coil has the advantage of creating relatively easily a magnetic field over a large area. However, it generates a homogeneous magnetic field which on its own will not act on the particle since the magnetomotive force is proportional to the gradient of the field (equation (9)). Still, the force is also proportional to the field suggesting that increasing the overall magnetic field will increase the force.

The aim of my work is to study the effect of adding a homogeneous field to the current technique of magnetomotive ultrasound (figure 6) and study the possible increase of the contrast agent displacement. This increase in displacement will benefit magnetomotive ultrasound imaging by improving the detection ability. With a greater displacement, particles further away from the magnet can be detected.

1.3 Course of Action

First, the problem was studied from a theoretical point of view. The theoretical model aimed at ascertaining the feasibility of the project and was based on already existing models. The theory defined different parameters of the experiments.

Then, a Helmholtz coil was built with dimensions based on what the theory provided. The coil performances were assessed and compared to the model. The practical part of the project revolved mainly around measuring the displacement of magnetic particles embedded in a phantom using magnetomotive ultrasound. The effect of adding the Helmholtz coil was studied for different parameters.

Last, in an attempt to take into consideration clinical constraints, a different version of the set-up was tried.

2 Method

This section details the theory developed to better understand the effect of adding the coil. The chapter describes the material and equipment used, the way the measurements were performs and how the data was analysed.

2.1 Theory

2.1.1 Magnetic field

A Helmholtz coil can produce a nearly homogeneous magnetic field over a large area. The particularity of a Helmhotlz coil is that the distance between the two parts of the coil is equal to the radius of the coil. For instance, for a coil of radius a, the distance between the coils is also a. The magnetic field varies only 0.1% at a distance 0.17a from the middle of the coil and 5% at a distance of 0.5a, *i.e.* inside one of the coils (Restrepo-Alvarez et al. 2012). More precisely, according to the Bio-Savart law, n turns of wire of radius R, supplied with a current I will generate a magnetic field of intensity:

$$B_1(x) = \frac{\mu_0 n I R^2}{2(R^2 + x^2)^{3/2}} \tag{10}$$

with x being the distance from the center of the Helmholtz coil. At the center, the magnetic field intensity is:

$$\begin{aligned} B_0 &= 2B_1(\frac{R}{2}) \\ &= (\frac{4}{5})^{\frac{3}{2}} \frac{\mu_0 n I}{R} \end{aligned} \tag{11}$$

The other magnetic field to take into account is created by a permanent magnet. The expression of the field from a magnetic dipole in cylindrical coordinates, for a distance r much greater than the size of the dipole, the so-called dipole approximation, is (Kraftmakher 2007):

$$\overrightarrow{B} = \frac{\mu_0 m}{4\pi r^3}(2cos(\theta)\overrightarrow{e_r} + sin(\theta)\overrightarrow{e_\theta}) \tag{12}$$

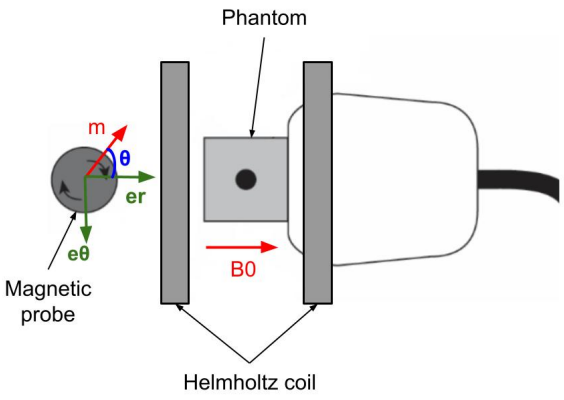

Figure 7: Drawing of the set-up showing the cylindrical frame of reference.

with m the magnetic moment and r and θ the cylindrical parameters.

The hypothesis that $B_z = 0$ is made, with z the axis perpendicular to the sheet surface pointing into the figure. The magnetic field is time-varying with a variation given by the angle $\theta = \omega t = 2\pi f t$ with ω the rotation frequency and f the frequency.

Taking the logarithm of the magnetic field expression along the axis e_r (equation (12)) results in an affine function:

$$log(B) = log(\frac{\mu_0 m}{2\pi}) - 3log(r) \tag{13}$$

2.1.2 Magnetomotive force

The particles embedded in the tissue, under the action of a magnetic field, will be subject to the magnetomotive force expressed as follow (Shevkoplyas et al. 2007):

$$F_m = \frac{\chi V}{\mu_0}(B \cdot \nabla)B + \rho V \nabla(M_0 \cdot B) \tag{14}$$

with, χ the magnetic susceptibility, V the volume of particles, B the magnetic flux density, M_0 the remanent magnetization and ∇ the gradient operator. This formula is valid for a weak magnetic field, *i.e.* when the magnetization depends linearly on the magnetic field as described in equation (5). When using superparamagnetic particles, as it is the case here, the remanent magnetization is 0, thus simplifying the force expression to the first term.

As a first approximation, the magnetic field from the permanent magnet will be expressed in Cartesian coordinates as one time varying component along the z axis, *i.e.* the axis going from the probe to the phantom (J. H. Oh 2006):

$$\overrightarrow{B}(x,y,z,t) = sin(2\pi ft)B_z(z)\overrightarrow{z} \tag{15}$$

Taking the homogeneous magnetic field from the coil along the z axis, the combined magnetic field is:

$$\overrightarrow{B}(x,y,z,t) = sin(2\pi ft)B_z(z)\overrightarrow{z} + B_0\overrightarrow{z} \tag{16}$$

Now using equation (14) and (16), the expression of the force along the z axis is:

$$F_{mz} = \frac{\chi V}{2\mu_0}(1 - cos(4\pi ft))B_z(z)\frac{\partial B_z}{\partial z} + \frac{\chi V}{\mu_0}sin(2\pi ft)\frac{\partial B_z}{\partial z}B_0 \tag{17}$$

Equation (17) shows that the addition of a homogeneous magnetic field will indeed contribute positively to the magnetomotive force. As expected, the force acting on the particles is twice the excitation frequency (J. Oh et al. 2006). This feature is used to eliminate unwanted frequency components that arise due to environmental noise. However, the homogeneous field will contribute to the force only every two periods since its frequency is not doubled. To keep the frequency doubling feature, the idea of having a time-varying homogeneous field was suggested. In this case, the combined magnetic field is:

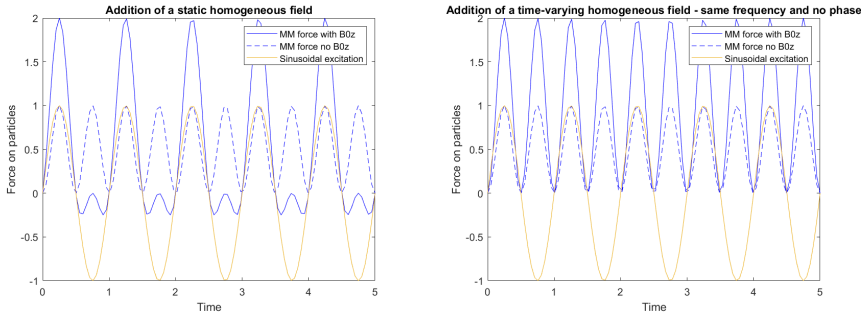

Figure 8: Comparison of the magnetomotive force when the homogeneous magnetic field is time-varying (right) and static (left).

$$\overrightarrow{B}(x,y,z,t) = sin(2\pi ft)[B_z(z) + B_0]\overrightarrow{z} \tag{18}$$

Thus, the magnetomotive force acting on the particles is:

$$F_{mz} = \frac{\chi V}{2\mu_0}\frac{\partial B_z}{\partial z}(1 - cos(4\pi f_n t))[B_z + B_{0z}] \tag{19}$$

This time, the contribution of the homogeneous field has the same frequency as the contribution from the permanent magnet. Figure 8 shows a comparison of the two cases.

Using the magnetic field expression of a dipole (equation (12)), a more precise expression of the magnetomotive force can be computed. The previous expression only described one component of the force and thus only one direction of movement. It was found that the movement is in fact elliptical (Evertsson et al. 2019) and thus another model is needed. Using cylindrical coordinates, two components of the force are taken into account for a better description of the problem. Equation (12) describes the field all around the magnet. Rotating the magnet amount to the same as going in a circle around it, *i.e.* making the angle θ vary in time while keeping the distance r constant.

Combining the magnetic field according to the coordinates shown in figure 7 gives:

$$\begin{cases} B_r &= (\frac{\mu_0}{2\pi r^3}m + B_0)cos(\theta) \\ B_\theta &= \frac{\mu_0}{4\pi r^3}msin(\theta t) \end{cases} \tag{20}$$

Using equation (14), the magnetomotive force is expressed with its two components:

$$\begin{cases} F_{m,r} &= -k[(\frac{\mu_0 m}{4\pi})^2 \frac{1}{r^7}(\frac{1}{2}(15 + 9cos(2\theta))) + \frac{\mu_0 m}{4\pi}\frac{1}{r^4}B_0(\frac{5}{2}(1 + cos(2\theta)))] \\ F_{m,\theta} &= -k[(\frac{\mu_0 m}{4\pi})^2 \frac{1}{r^7}(\frac{5}{2}sin(2\theta)) + \frac{\mu_0 m}{4\pi}\frac{1}{r^4}B_0(\frac{3}{2}sin(2\theta))] \end{cases} \tag{21}$$

The equations describe an elliptical path for the force, suggesting also an elliptical path for the particles, as observed during experiments (Evertsson et al. 2019). The homogeneous magnetic field adds a term to the magnetomotive force expression predicting an increase in displacement. In addition, the increase happens on both components of the force. The circular path of the particle should show a greater diameter when adding the homogeneous field.

2.1.3 Induced current

If the coil is not supplied with any current, an induced current will be created by the magnetic probe. This induced current will generate a magnetic field which opposes the one from the magnetic probe as described by Faraday's law of induction:

$$e = -n\frac{d\phi}{dt} \tag{22}$$

with e the electromotive force, n the number of turns in the coil and ϕ the magnetic flux given by:

$$\phi = \iint \overrightarrow{B}.\overrightarrow{n}\,\mathrm{d}S \tag{23}$$

Using the simple expression $B_{magnet} = Bcos(\omega t)$ to describe the magnetic field, the electromotive e can be expressed as :

$$\begin{aligned} e &= -n\frac{d}{dt}(B\pi R^2 cos(\omega t)) \\ &= nB\pi R^2 \omega sin(\omega t) \end{aligned} \tag{24}$$

Then, as the magnetic field from the coil is given by equation (10), by substituting the current by the electromotive force divided by the resistance of the coil R_Ω, the expression of the total magnetic field amplitude in the middle of the coil is:

$$B_{tot} = B[1 - (\frac{4}{5})^{\frac{3}{2}} \frac{\mu_0 n^2}{R_\Omega} \pi R\omega] \tag{25}$$

The total magnetic field amplitude B_{tot} is indeed lower than the amplitude of the field from the magnetic probe B.

2.1.4 Heating in the coil

An important consideration for the design of the coil is the heat it will generate. This part will deal with thermal considerations and the influence of the different parameters of the coil's design.

The power dissipated by the coil is equal to the increase rate of internal energy plus the rate of energy transferred to the surroundings through its surface S (Fontanet et al. 2019).

$$P = R_\Omega I^2 = mc_{coil}\frac{dT}{dt} + h_c S\Delta T \tag{26}$$

with R_Ω the electrical resistance, I the current, m the mass of the coil and c_{coil} the heat capacity of the coil. The heat exchange term was estimated using Newton's law of cooling, thus taking into account h_c the convective heat transfer coefficient and ΔT the temperature difference between the coil and the surrounding air. (Fontanet et al. 2019) solves the equation in the case of a stationary regime. However, to have a better understanding of

the coil's behavior, the transitory regime will be considered in this study. In addition, the current is alternating to give a time-varying magnetic field, *i.e.* $I = I_0 cos(\omega t)$. Solving equation (26) is solving the first order differential equation:

$$\frac{dT}{dt} + \omega_0 T(t) = \omega_0 (\frac{1}{2} T_I + T_0 + \frac{1}{2} T_I cos(2\omega t)) \tag{27}$$

T_I and ω_0 can be expressed with the physical properties of the coil, *i.e.* D_w the wire diameter, ρ the density of the material used to make the coil and ρ_{el} its resistivity.

$$\begin{cases} \omega_0 = \frac{h_c S}{mc} = \frac{4h_c}{\rho D_w c} \\ T_I = \frac{R_\Omega I_0^2}{h_c S} = \frac{\rho_{el} 4 I_0^2}{h_c \pi D_w^3} \end{cases} \tag{28}$$

Solution to equation (27), which gives the temperature in the coil, is:

$$T(t) = \frac{T_I}{2}[1-(1+\frac{1}{4\frac{\omega^2}{\omega_0^2}+1})e^{-\omega_0 t}+\frac{1}{4\frac{\omega^2}{\omega_0^2}+1}(cos(2\omega t)+2sin(2\omega t))]+T_0 \tag{29}$$

To solve the equation, the initial condition was taken as $T(t=0) = T_0$.

2.2 Material and Equipment

The Helmholtz coil was handmade and aimed at reaching a field of 0.01 T as this value should give a significant increase in force according to the math model (equation (21)). The radius was chosen as 0.045 m to fit the phantom and the ultrasound probe inside the coil. For the current intensity to remain relatively small, the number of turns for each coiling is 150. The copper wire has a diameter D_w of 1.3 mm to prevent the coil from heating too much and was set around a Plexiglas tube in an orthocyclic winding layout of 8 layers composed of a decreasing number of rows from 22 to 15. Each layer was glued together and fitted on the row below to form a pyramidal shape. The resistivity of copper ρ_{el} is 1.72×10^{-8} Ω.m, its density ρ_{copper} = 8960 kg.m^{-3} and its specific heat c = 385 J.K^{-1}.kg^{-1}

The convective heat transfer coefficient was taken as $h_c = 10$ W.m^{-2}.K^{-1} (Fontanet et al. 2019).

The images were taken using the VisualSonics Vevo F2 together with the ultrasound probe L38xp which has a transmission frequency of 7.1 MHz. Each cine-loop were 150 frames acquired with a 48MHz sample frequency. The focus was set to 25 mm, right under the insert in the phantom. The RF data collected by the scanner was exported and treated using Matlab on a computer.

Magnetic field measurements were performed using the Three Axis Hall Magnetometer THM1176 from Metrolab Technology SA, Switzerland. The probe was controlled using a Matlab algorithm and homemade script combined with pre-build Matlab function from Metrolab. Measurements of the magnetic field were taken with a sampling frequency of 13 Hz and then reconstructed using the *resample* function from Matlab with a reconstruction factor of 6. In case of magnetic field intensity measurements over distance or phase difference, the field was measured for 5 seconds for each field value. Then, the algorithm reconstructed the signal with *resample* and took the mean value of the local maxima. The algorithm also allowed for real-time measurements.

2.3 Practical experiments

One main experimental set-up was used to measure the magnetic field and the displacement. The magnetic probe was placed outside of the Helmholtz coil, aligned with the coil's axis and either the magnetometer or the phantom which was placed inside of the coil. In the case of displacement measurements, the ultrasound probe was added in contact to the phantom's surface through the coil (Figure 9 and 12). From there, the distance between the magnetic probe and the phantom's edge could be increased while keeping the vertical alignment, thanks to the translation stage on which the magnetic probe was mounted.

The magnetic probe is composed of a neodymium magnet (K&J magnetics, USA) set in rotation by a motor (DCX 22 S, maxon motor, Switzerland). The motor was connected to a 20 V power supply (PSI 8080-60 T, Elektro-Automatik GMBH & CO. KG, Germany) and controlled from a personal computer using the program EPOS Studio 3.3. The permanent magnet rotated at 300 rpms to generate a 5 Hz oscillation of the magnetic field.

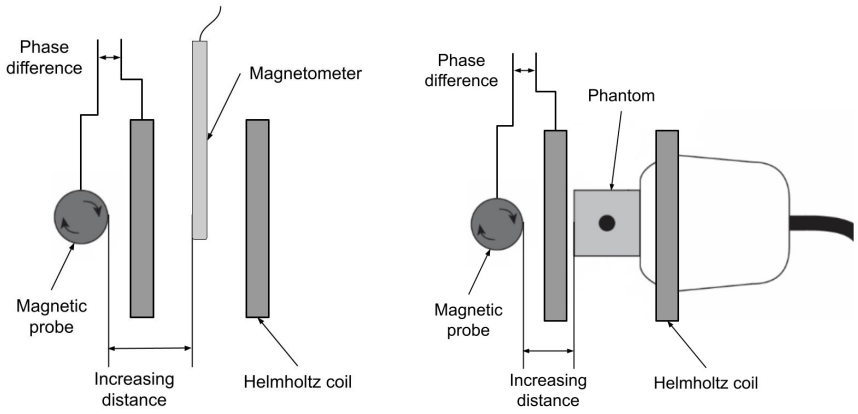

Figure 9: Left: Drawing of the experimental set-up for the magnetic field measurements. The magnetometer probe is in the middle of the coil and take measurements along the direction of the magnetic field from the coil. Right: Drawing of the experimental set-up for the displacement measurements showing the phantom and its inclusion of particles as well as the ultrasound probe used to take images.

For the coil power supply, the function generator (33120 A, HP Inc, USA) generated a 5 Hz sinusoidal signal of 100 cycles when triggered by a rising slope of the sinusoidal signal from the magnetic probe. The number of cycles was chosen to produce a smooth signal as the function generator tended to miss a few triggers. With a 100 cycles, the signal was continuous for at least 20 seconds. A phase difference with the triggering signal could be set within the parameters of the function generator. The signal was then sent to the amplifier (EP4000 Europower, Berhinger, Germany) before reaching the coil. Both signal from the magnetic probe and the amplifier were monitored on the oscilloscope (TBS 1052C, Tektronix, USA) (Figure 10).

The set-up previously described works well for academic research but would be difficult to translate into clinical practice. Therefore, another disposition of the elements was tried which could be more easily applicable to real life application. The phantom containing the magnetic particles was moved out of the Helmholtz coil and the other elements were kept the same (figure 11 and 13). The particles were set 2.5 mm away from the edge of the Helmholtz coil which was given a 500 mV signal amplified with 30dB. The magnetic field was 15 mT inside the coil and 6 mT where the particles were.

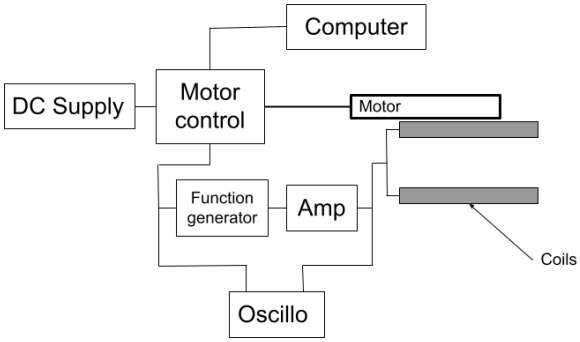

Figure 10: Drawing of the power supply for the magnetic probe and the Helmholtz coil. The signal sent to the motor is used to trigger the function generator which creates the signal sent to the coil.

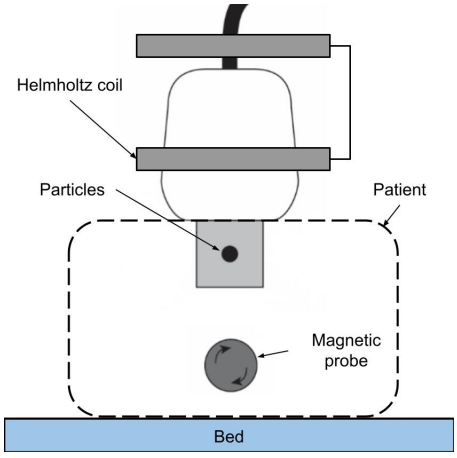

Figure 11: Experimental set-up when the particles are outside the coil.

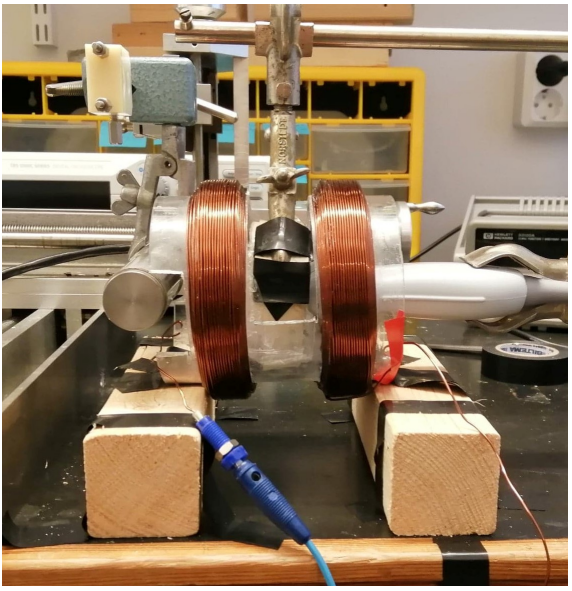

Figure 12: Picture of the experimental set-up showing from left to right: the magnetic probe, the Helmholtz coil, the phantom and the ultrasound probe.

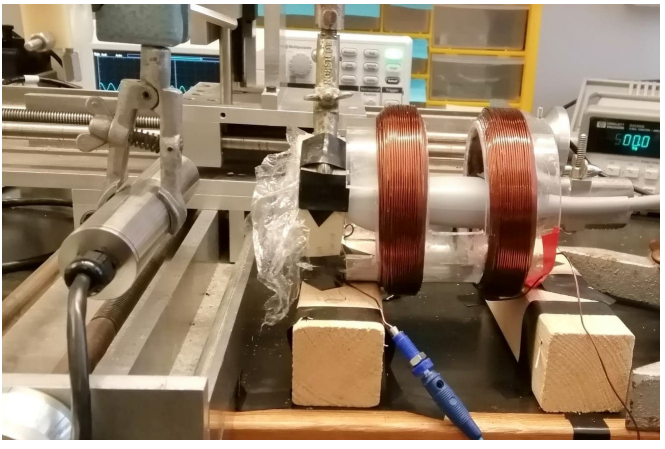

Figure 13: Picture of the experimental set-up with the phantom outside the coil showing from left to right: the magnetic probe, the phantom and the ultrasound probe inside the Helmholtz coil.

2.4 Data analysis

The data collected by the ultrasound scanner was exported to a personal computer and processed using Matlab. Different programs came into action to extract the displacement values of the particles inside the phantom under the action of the magnetic field.

The RF data exported from the ultrasound scanner was stored in binary files and the parameters of sequence were stored in .xml files. An algorithm extracted the data from the binary files and performed a Hilbert transform before storing the converted data in a Matlab array. The process converts the RF data into IQ data. The parameters of importance were read in the corresponding .xml files and added to the Matlab array.

The displacement in each cine-loop was evaluated using an algorithm developed by Maria Evertsson et al. 2013. It was found that the displacement outside particle-laden regions can have displacement but that this displacement has a phase shift of approximately π. In addition, as shown previously, the particles move at twice the excitation frequency whereas surrounding tissues move at the excitation frequency. Thus, the program used the IQ data to perform quadrature detection and phase gating at the frequency at which the particles within the phantom are moving, thus filtering out the other frequencies caused by noise. The algorithm produced an image showing the displacement with a color bar superimposed on the B mode image.

Then, the mean displacement was calculated over a region of interest (ROI) from the images previously created.

The whole process of analysing the data was facilitated to treat a large amount of data from the scanner with an algorithm making the link between the different algorithms (Figure 14). The images are cropped manually to select only the insert in the phantom. The frequency for the quadrature detection and the phase gating can be adjusted and corresponds to the frequency of motion of the particles, *i.e.* twice the frequency of excitation. More details on this program are given in appendix A.

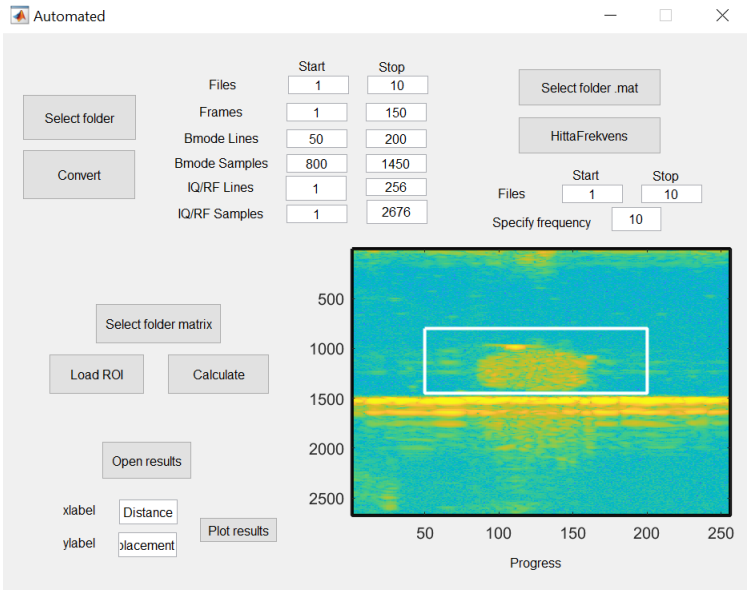

Figure 14: Graphical User Interface (GUI) to facilitate the data analysis from the RF data out of the scanner to the displacement measurement over a ROI.

3 Results

Both theoretical expectations and experimental results are presented in this section. At first, the performance of the coil, regarding heating and magnetic field generation, are given. Then, the different results from displacement measurements are shown.

3.1 Theory

3.1.1 Heating

The heating of the coil was predicted using equation (29) for the range of current 1 A to 9 A which is the working range of the coil and the predictions were compared to experimental temperature measurements over a five minutes time span (figure 15). For a 9 A current, which corresponds to 20 mT for the coil, the temperature increase after 5 minutes is 25 °C which is 12 °C less than what was expected from theory.

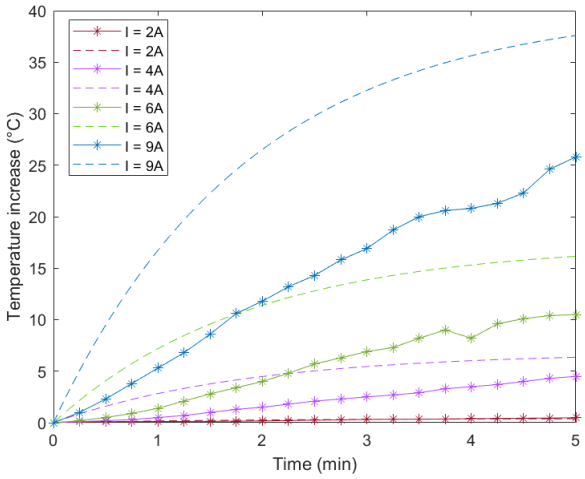

Figure 15: Temperature increase in the Helmholtz coil over time for different values of current showing theoretical predictions (dash lines) and experimental measurements (solid lines).

3.1.2 Magnetic field of a magnetic dipole

The logarithm of the magnetic field shows a linear relationship with the logarithm of the distance over the range of length: 25 mm to 60 mm and 70 mm to 110 mm (figure 16). A linear fit was performed on each plot, showing a dependency in one over the distance squared for the first range (25 mm to 60 mm) and a dependency in one over r to the power of three for the second range of distances (70 mm to 110 mm).

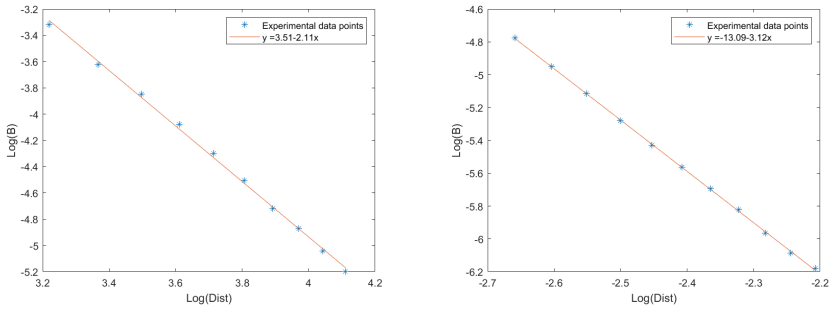

Figure 16: Logarithm of the magnetic field as a function of the logarithm of the distance Left: for the range 25 mm to 60 mm. Right: for the range 70 mm to 110 mm.

3.1.3 Theoretical predictions

The results presented in this section were obtained using equation (21) and are consequently only graphical representation of the mathematical expression.

As described in the method section, the model describes a circular path of the force and this path is increased along the axial and along the radial direction when the homogeneous field is added (figure 17). The two components of the force increase linearly with the strength of the homogeneous field (figure 18). When plotted as a function of the distance between the magnet and the particle, the force is greater with the added homogeneous field.

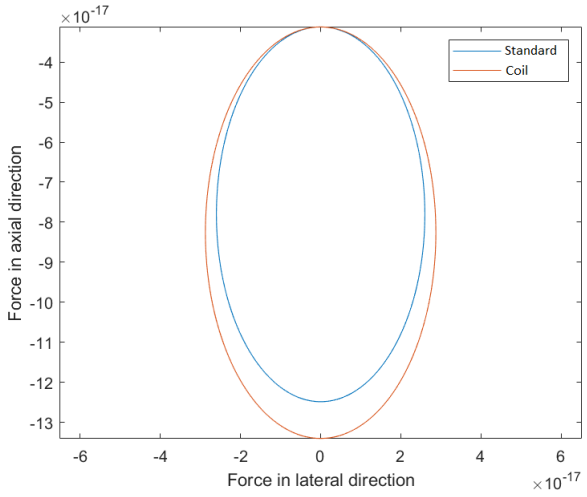

Figure 17: Magnetomotive force path for a homogeneous field intensity of 30 mT at a distance of 1cm from the magnetic probe.

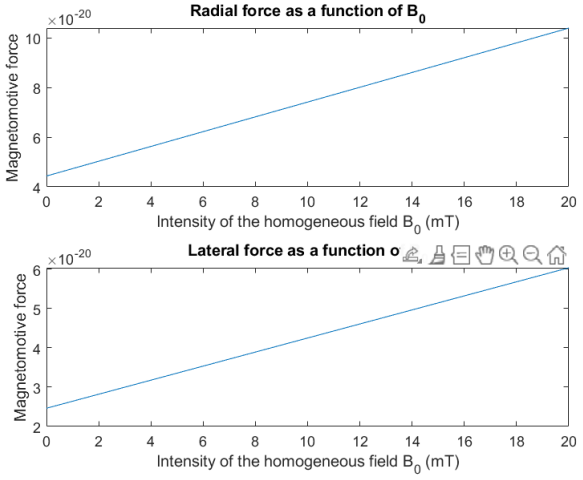

Figure 18: Magnetomotive force as a function of the homogeneous magnetic field at a distance of 5 cm from the magnetic probe.

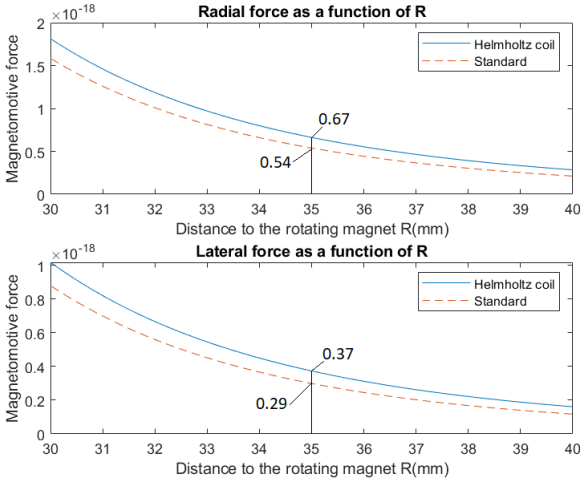

Figure 19: Magnetomotive force as a function of the distance between the magnetic probe and the particles for a 10 mT homogeneous magnetic field.

3.2 Experiments

3.2.1 Magnetic field of the Helmholtz coil and coupling of the magnetic fields

The characteristics and performance of the homemade Helmholtz coil are evaluated and shown in this section.

The relationship between the voltage and the current is given by Ohm's law. First, the coil is supplied with DC current to compare its performance with theory (equation (10)). Using the results from figure 20 the resistance of the coil was measured: R_Ω is 2.17 Ω. The empirical relationship between the magnetic field generated by the coil and its supplied DC current is $B_{exp} = 0.0025I$ (figure 21). From the theory described in section 2.1.1, the relationship between current and magnetic field is $B_{theo} = 0.003I$.

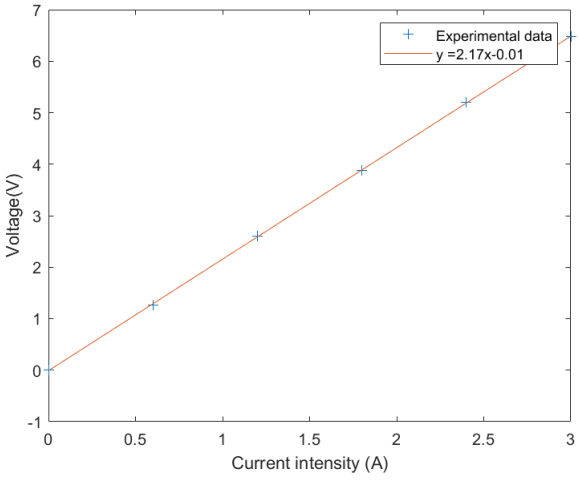

Figure 20: Voltage in the coil as a function of the supplied DC current.

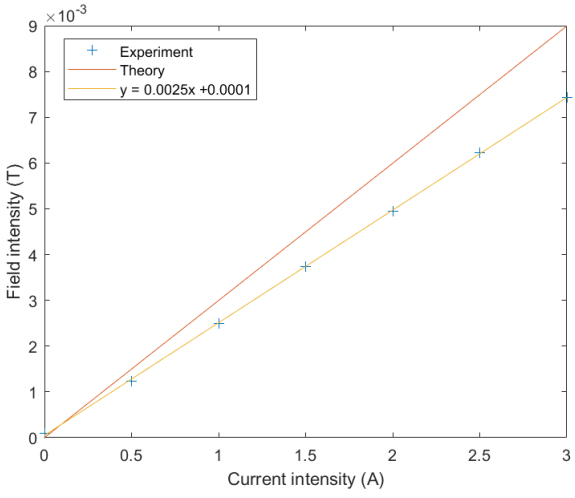

Figure 21: Magnetic field intensity generated by the coil as a function of the supplied DC current.

When supplied with AC voltage, the magnetic field intensity from the coil is given by $B_{exp/AC} = 0.001V$ (figure 22). To express this relation with the current as in the case of the DC supply, one should consider the inductance L of the coil:

$$V = \sqrt{R^2 + (L\omega)^2}I \tag{30}$$

Thus, using the measurements performed with DC current, the inductance was computed: $L = 0.04$ H.

As both magnetic fields vary in time, they add-up or subtract depending on the phase difference between them. Figure 23 shows that the fields add-up and reach the highest intensity for a phase difference of 120°.

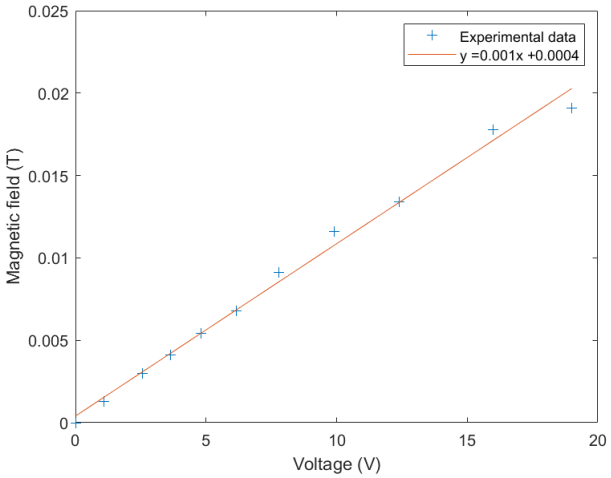

Figure 22: Magnetic field intensity generated by the coil as a function of the supplied AC voltage.

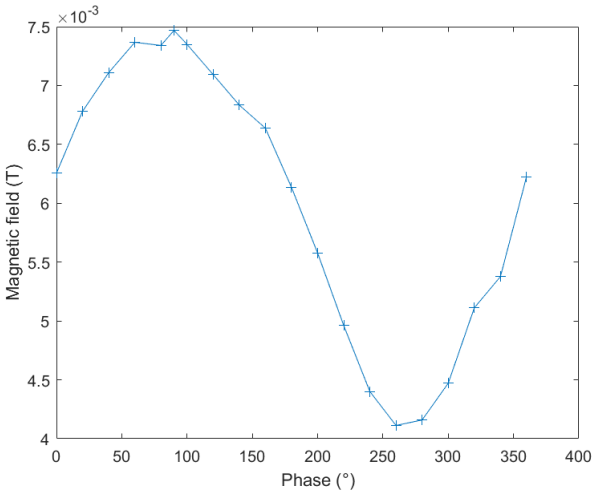

Figure 23: Magnetic field intensity as a function of the phase difference between the electrical signals sent to the Helmholtz coil and the magnetic probe.

The magnetic field intensity was measured as a function of the distance between the magnetometer and the magnetic probe in three different cases: set-up without the coil (only the magnetic probe), set-up with the coil but without current and the coil with current (figure 24). The magnetic field from the Helmholtz coil was measured separately and has an intensity of 6 mT. The theoretical values for the case 'coil on' were expressed as: $B_{theo} = B_{magnet} + B_{coil}$. For the case 'coil off', equation (25) was used.

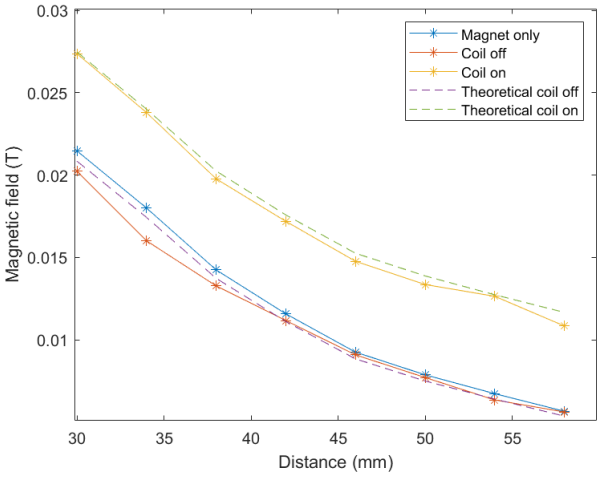

Figure 24: Theoretical and experimental magnetic field intensity in the case of the magnetic probe only, the coil without current (coil off) and the coil supplied with current (coil on).

3.2.2 Displacement as a function of distance

The displacement was measured as a function of the phase difference between the signals sent to the coil and to the magnetic probe. The shape of the magnetic field for the same difference is also plotted (figure 25). Similarly to the magnetic field, the displacement reaches a maximum and a minimum over the 360 possible degrees of phase difference between the signals.

For the three same conditions as the magnetic field measurements, the displacement is measured as a function of the distance between the magnetic probe and the phantom (figure 26). The displacement is twice as large when using the coil at a distance of 25 mm. At 53 mm, the increase is of 40%.

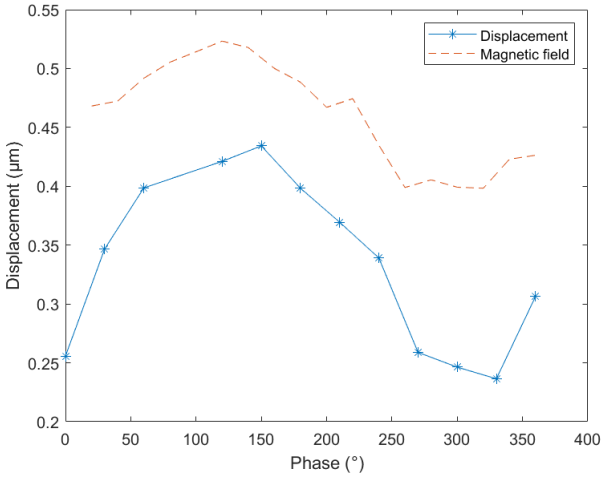

Figure 25: Displacement as a function of the phase difference between the signals sent to the coil and to the magnetic probe. The shape of the magnetic field as a function of phase is represented with a dash-line.

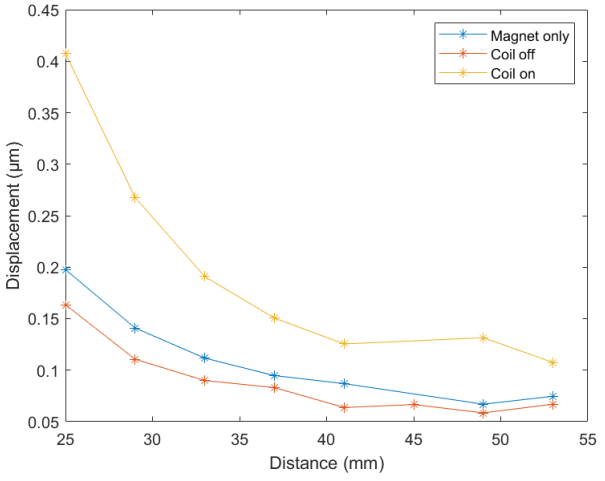

Figure 26: Displacement as a function of the distance between the magnetic probe and the phantom.

3.2.3 Displacement as a function of the magnetic field

The displacement increases with the magnetic field strength of the field generated by the coil (figure 27). The displacement measurements were made for a distance between the magnetic probe and the phantom of 35 mm and 50 mm.

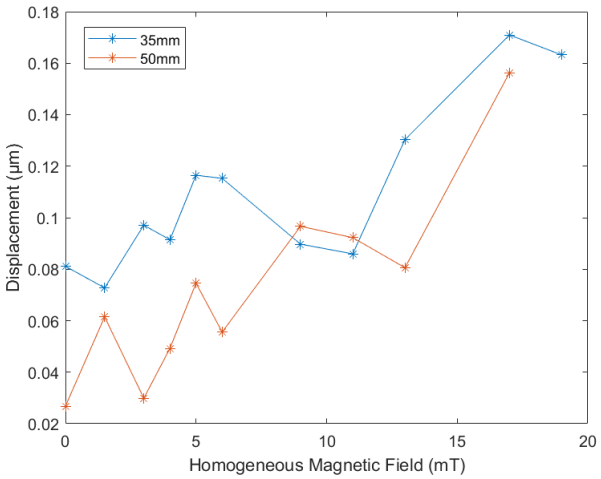

Figure 27: Displacement as a function of the homogeneous magnetic field generated by the Helmholtz coil for distances between the magnetic probe and the phantom of 35 mm and 50 mm.

3.2.4 Lateral displacement as a function of distance

The theory suggests that the lateral motion is also increased by the addition of the homogeneous magnetic field. Moving the ultrasound probe to look at the phantom from the top, the lateral displacement was measured and increased with the strength of the homogeneous magnetic field (figure 28).

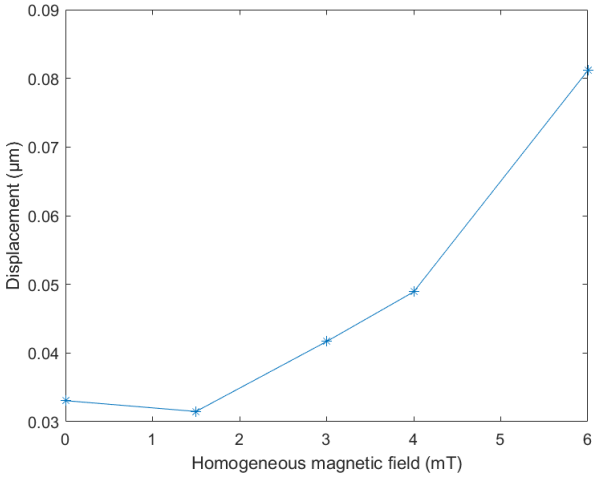

Figure 28: Displacement in the lateral direction as a function of the magnetic field generated by the Helmholtz coil.

3.2.5 Particles outside the coil

In the case of the particle outside of the coil, an increase in displacement was also measured when adding the coil (figure 29). The measurements start with the magnetic probe 27 mm away from the phantom.

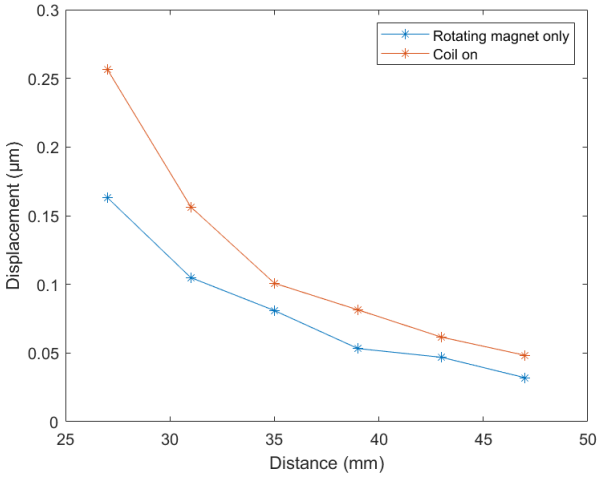

Figure 29: Displacement as a function of the distance between the magnetic probe and the phantom when the particles are outside of the coil.

4 Discussion

This chapter discuss the results displayed previously regarding the theoretical expectations, the coil performances and the measured displacement of particles inside the phantom.

4.1 Theory

As a function of the distance between the rotating magnet and the magnetic particles, the theoretical magnitude of the force ranges between 10^{-16} and 10^{-18} N. This is in accordance with the results obtained by J. H. Oh 2006 from which the value of k is taken. The numerical values corresponds to SPION, *i.e.* nano-particles whereas the phantom used during the experiments has an inclusion made of micro-sized particles which can explain some of the differences between experimental measurement and theory.

The magnetic field generated by a magnetic dipole decreases with the distance to the power of three (equation 12). However, according to the experiments, this behaviour is only observed 7 cm away from the magnet (figure 16 right) whereas at a closer range, the decrease scales inversely with the distance to the power of two (figure 16 left). As this expression is used to derive the magnetomotive force, the predicted decrease of the magnetomotice force, proportional to the inverse of the distance to the power of seven, is only valid at a great distance from the magnet.

In the expression of the magnetomotive force (equation (21)), the term including the homogeneous field strength B_0 scales with the inverse of the distance to the power of four whereas the other term is proportional to the inverse of the distance to the power of seven. Consequently, when increasing the distance, the role played by the homogeneous field becomes more important. Still, the experiments did not show clearly this scaling of the different components of the force. The increase from the addition of the coil was not more important at greater distances.

4.2 Coil performances

The coil was handmade and attesting that its actual behaviour relates to the model was a critical point. The measurements also allowed to define

important parameters such as the relationship between the magnetic field and the current or voltage. Some loss, probably due to heating, occurs in the coil but the performance are satisfactory and were sufficient to generate the homogeneous magnetic field.

Still, a limit of the coil is the heat it produces. The theoretical model gives a rough approximation of the temperature increase. The gap can be explained by the limits of the derivation and by the limits of the experiment. The theory relies on Newton's law of cooling describing the convective exchange of heat between the coil and air. The convective coefficient h_c is difficult to evaluate. A value from an article describing a similar case was used (Fontanet et al. 2019). The surface of heat exchange was chosen as the shell of the cylinder created by the coiling. In reality, there is also air within the coiling and part of the coil is in contact with the Plexiglas support resulting in a conductive heat exchange. As for the experiment, the coupling between the thermometer and the coil was realised using ultrasound gel. This thermal coupling is not optimal and probably induced inertia as the gel had to heat up as well.

The different parameters of the coil were determined to achieve a magnetic field of 10 mT to 20 mT as such values would result in an increased displacement according to the theoretical model. The coil also had to comply to geometrical consideration related to the size of the phantom or the size of the ultrasound probe. As a result, for future experiments, a better optimization of the radius, the number of turns and the diameter of the wire will reduce the needed current and the resulting heating.

4.3 Increased displacement

Both results from the measurements of the magnetic field and the displacement show the crucial role played by the phase. The displacement follows the behaviour of the magnetic field. All the measurements involving the Helmholtz coil were made after determining the best phase difference value to set in the function generator. Indeed, this value is not absolute but relative to the position of the magnet and the coil. For example, turning the coil upside down shifts the optimal phase difference value by 90°.

The magnetic field amplitudes from both fields add up nicely when the right phase difference is found. As predicted from theoretical consideration, the total magnetic field is reduced by the coil without current, illustrating

Faraday's law of induction. Consequently, with the reduced magnetic field, the displacement is also reduced. When the coil is supplied with current, there is indeed a increase in the displacement. The displacement reached at a 25 m depth when using only the magnetic probe is now reached at a 33mm depth, increasing the penetration of magnetomotive ultrasound by 8 mm for a 6 mT homogeneous field. The displacement increases with the homogeneous field intensity, suggesting that the penetration could be even more increased. Nonetheless, the relationship between the displacement and the homogeneous field strength was thought to be linear, the same way the magnetomotive force relates to the homogeneous field strength. From the results, this relation can not be clearly established. Moreover, the theoretical model predicted an increase in the force both in the axial and lateral direction. This prediction was observed experimentally with the increase of the displacement in both directions.

When adding the coil, a practical challenge is to keep a smooth rotation of the permanent magnet in the magnetic probe. The field generated by the coil disrupts the rotation and distort the signal in the motor. In addition, the elements of the set-up shakes a lot. The initial distance between the phantom and the magnetic probe thus couldn't be taken too small to limit the shaking and disruption of the rotation. Putting the particles outside the coil, in addition to its practical aspects, had also the advantage of allowing a greater distance between the coil and the motor. Even though the experiment was out of the theoretical model validity since at this range, the field from the coil is not homogeneous anymore, it also showed an increase in the displacement. Another set-up was imagined with the Helmholtz coil in the bed. However, this entailed that the permanent magnet was between the coil and the phantom. Given the magnitude of the respective magnetic field from the magnetic probe and the coil, this set-up was not tried as it wouldn't have shown any effect when adding the coil.

Another way of adding the coil was considered. Instead of aligning the phantom, the magnetic probe and the coil, the latter is rotated by 90°. This model was described theoretically and drawings and equations are given in the appendix B. No experimental experiments were performed as the theoretical consideration suggested a decrease of the magnetomotive force.

5 Conclusion

The theoretical model developed in this report suggests an increase in displacement when adding a homogeneous field. This increase was indeed observed experimentally, establishing a proof of concept.

The model showed some limits and the link to the experiments is not clear yet as a few steps are still missing to describe properly the theoretical displacement. Similarly, the experiments can be pushed further with higher magnetic field strength and different dispositions for the elements involved.

The work conducted in this report shows that adding a homogeneous magnetic field in magnetomotive ultrasound increases the displacement both axially and laterally thus pointing to a way to improve the sensitivity in magnetomotive ultrasound by adding a homogeneous magnetic field.

References

Mulvana, Helen et al. (Jan. 2017). 'Characterization of contrast agent microbubbles for ultrasound imaging and therapy research'. In: *IEEE Transactions on Ultrasonics, Ferroelectrics, and Frequency Control* 64 (1), pp. 232–251. ISSN: 08853010.

Dréan, Antonin et al. (Aug. 2019). 'Temporary blood–brain barrier disruption by low intensity pulsed ultrasound increases carboplatin delivery and efficacy in preclinical models of glioblastoma'. In: *Journal of Neuro-Oncology* 144 (1), pp. 33–41.

Barua, Sutapa and Samir Mitragotri (Apr. 2014). 'Challenges associated with penetration of nanoparticles across cell and tissue barriers: A review of current status and future prospects'. In: *Nano Today* 9 (2), pp. 223–243.

Avril, N. et al. (2001). 'Glucose metabolism of breast cancer assessed by 18F-FDG PET: Histologic and immunohistochemical tissue analysis'. In: *Journal of Nuclear Medicine* 42 (1), pp. 9–16.

Tian, Jie (2013). *Molecular Imaging: Fundamentals and Applications.*

Cobbold, Richard (2006). *Foundations of Biomedical Ultrasound.*

Sjöstrand, Sandra (2021). *Magnetomotive ultrasound for nanomedicine a mechanistic approach to detection, evaluation and safety assessment.*

Sjöstrand, Sandra et al. (2018). 'Revolving Permanent Magnet for Magnetomotive Ultrasound'. In: *2018 IEEE International Ultrasonics Symposium (IUS).*

Sjöstrand, Sandra, Maria Evertsson and Tomas Jansson (Oct. 2020). 'Magnetomotive Ultrasound Imaging Systems: Basic Principles and First Applications'. In: *Ultrasound in Medicine and Biology* 46 (10), pp. 2636–2650.

Bao, Gang, Samir Mitragotri and Sheng Tong (July 2013). 'Multifunctional Nanoparticles for Drug Delivery and Molecular Imaging'. In: *Annual Review of Biomedical Engineering* 15, pp. 253–282.

Gupta, Ajay Kumar and Mona Gupta (June 2005). 'Synthesis and surface engineering of iron oxide nanoparticles for biomedical applications'. In: *Biomaterials* 26 (18), pp. 3995–4021.

Oh, Jung Hwan (2006). *Magneto-Motive Detection of Nanoparticles and Hemoglobin.*

Shevkoplyas, Sergey S. et al. (Sept. 2007). 'The force acting on a superparamagnetic bead due to an applied magnetic field'. In: *Lab on a Chip* 7 (10), pp. 1294–1302.

Pisani, Paola et al. (1999). 'Estimates of the worldwide mortality from 25 cancers in 1990'. In: *J. Cancer* 83, pp. 18–29.

Mulsow, J. et al. (June 2003). 'Sentinel lymph node mapping in colorectal cancer'. In: *British Journal of Surgery* 90 (6), pp. 659–667.

NanoEcho (2022). NanoEcho. URL: https://nanoecho.se/en/.

Wang, Hong-Wei, Huang Chih-Chia and Li Meng-Lin (2019). 'Improved Backward Mode Pulsed Magnetomotive Ultrasound via Pre-magnetization of Superparamagnetic Iron Oxide Nanoparticles'. In: *2019 IEEE International Ultrasonics Symposium (IUS)*.

Restrepo-Alvarez, Andres, Edinson Franco-Mejia and Carlos Pinedo-Jaramillo (2012). 'Study and analysis of magnetic field homogeneity of square and circular Helmholtz coil pairs: A Taylor series approximation'. In: *2012 Andean Region International Conference*.

Kraftmakher, Yaakov (May 2007). 'Magnetic field of a dipole and the dipole-dipole interaction'. In: *European Journal of Physics* 28 (3), pp. 409–414.

Oh, Junghwan et al. (Aug. 2006). 'Detection of magnetic nanoparticles in tissue using magneto-motive ultrasound'. In: *Nanotechnology* 17 (16), pp. 4183–4190.

Evertsson, M et al. (2019). 'Revolving permanent magnet causes rotating particle motion that makes new detection schemes possible in magneto-motive ultrasound'. In: *2019 IEEE International Ultrasonics Symposium (IUS)*.

Fontanet, A et al. (2019). 'Design and construction of 3D Helmholtz coil system to calibrate 3D Hall probes'. In: *10th Int. Particle Accelerator Conf.*

Evertsson, Maria et al. (2013). 'Frequency-and phase-sensitive magnetomotive ultrasound imaging of superparamagnetic iron oxide nanoparticles'. In: *IEEE Transactions on Ultrasonics, Ferroelectrics, and Frequency Control* 60 (3), pp. 481–491.

Appendix

A Automated.mat

The particle motion is extracted from the ultrasound images by a dedicated Matlab algorithm. This algorithm was designed to treat IQ data. As the ultrasound scanner exports RF data, another algorithm is used for conversion. Last, a third algorithm computes the mean displacement over a region of interest (ROI). All the algorithms run with a graphical interface but can treat only one cineloop at a time. As the experiment was repeated multiple times, a Matlab script was developed to perform more easily the whole process. The different parts of the Matlab script are described in this appendix.

The button 'Select folder ' on the top left opens a dialogue box. The user can select the folder where the data from the ultrasound scanner is saved. The images are loaded and their parameters are displayed in the boxes which can be edited and used to crop the image (figure 30). Once the settings are chosen, 'Convert' will launch the conversion of the data to readable Matlab file for the frequency analysis. When selecting the folder for saving the data, a name can be given to the files. Under the picture 'Progress' shows the progression of the algorithm.

The top right corner is dedicated to the frequency and phase analysis of the image and extracts the displacement. 'Select folder .mat' allows the user to select a folder where the converted files are stored (figure 31). The frequency to specify is twice the frequency of excitation. Clicking 'HittaFrekvens' starts the analysis. A phase window, used to discriminate between noise and actual particle movement, is chosen by the user for each image of the cineloop (figure 32). After this stage, a image showing the particle displacement is constructed (figure 33).

On the middle left is the section dedicated to computing the mean displacement over a ROI. The ROI is drawn on the picture thanks to another algorithm (figure 34) and then imported in the program (figure 35). 'Select folder matrix' and 'Calculate' select respectively the folder where the analysed data is and in which folder to save the results.

Last, the bottom left corner extracts the data from the .mat file saved at the previous step and plots the displacement. Labels are editable from the

graphical interface.

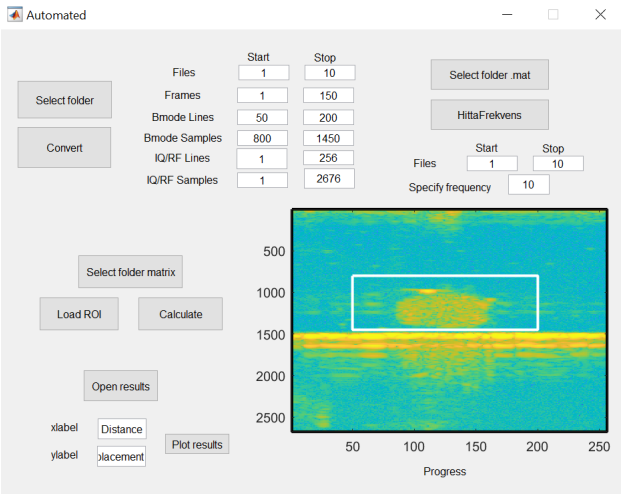

Figure 30: Images are loaded and their parameters is displayed before the conversion

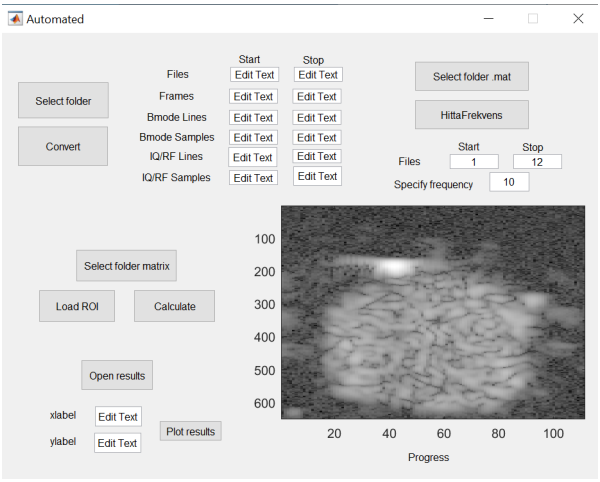

Figure 31: Selection of the number of analysed files and frequency for displacement computing.

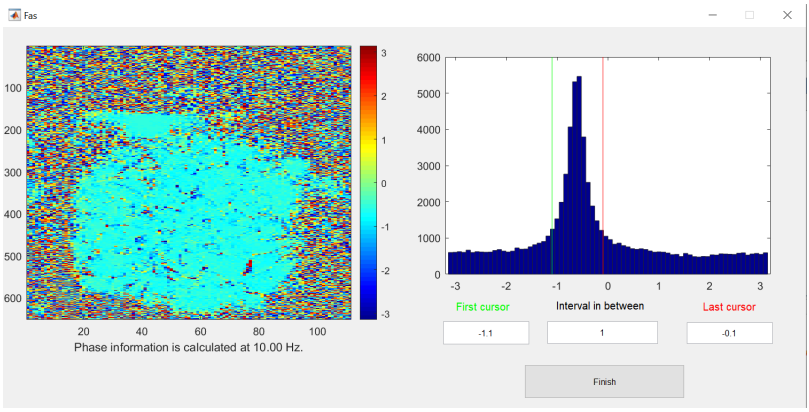

Figure 32: The user chooses the phase window for the quadrature detection and phase gating.

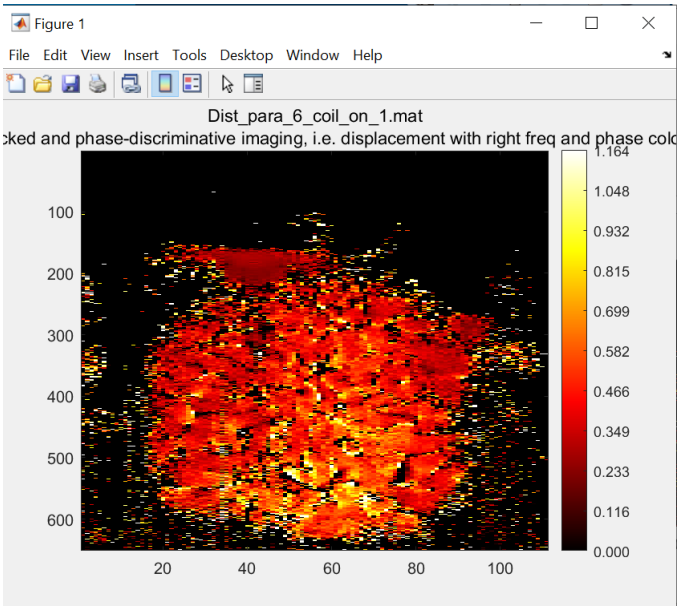

Figure 33: Image showing the displacement of particles inside the phantom after quadrature detection and phase gating.

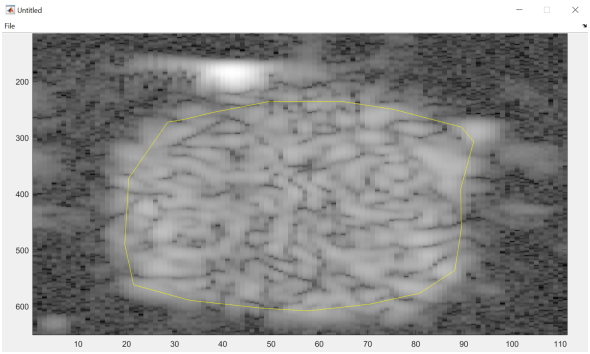

Figure 34: The ROI is drawn on the picture using a Matlab script.

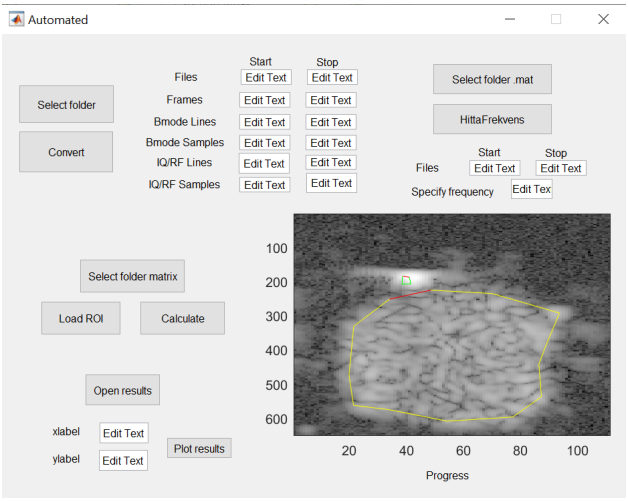

Figure 35: The mean displacement is computed over a ROI and save in a Matlab file.

B Perpendicular case

At an early stage of the project, the position of the coil in respect to the magnetic probe was discussed. Two ideas emerged, one is presented in the main part of the document and the other one is presented in this section.

In this case, the axis of the Helmholtz coil is perpendicular to the line drawn by the alignment of the magnetic probe, the phantom and the ultrasound probe (figure 36).

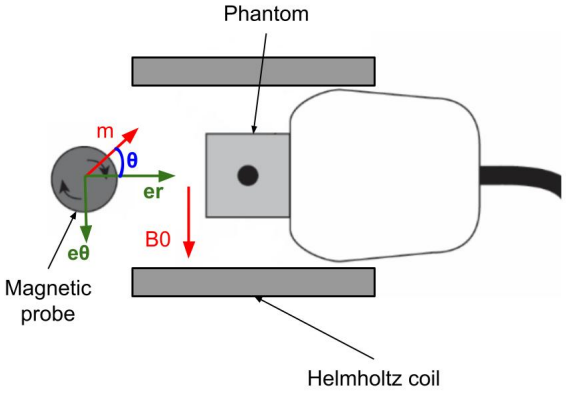

Figure 36: Drawing of the set-up showing the cylindrical frame of reference.

The combined magnetic field created by the magnetic probe and the Helmholtz coil is :

$$\overrightarrow{B} = \frac{\mu_0 m cos(\theta)}{2\pi r^3}\overrightarrow{e_r} + (\frac{\mu_0 m}{4\pi r^3} + B_0) sin(\theta)\overrightarrow{e_\theta} \tag{31}$$

Substituting equation (31) in the expression of the magnetomotive force :

$$\begin{cases} F_{m,r,\perp} &= -k[(\frac{\mu_0 m}{2\pi})^2 \frac{1}{r^7}(\frac{1}{2}(15+9cos(2\theta))) - \frac{\mu_0 m}{4\pi r^4} B_0(cos(2\theta)-1)] \\ F_{m,\theta,\perp} &= -k[(\frac{\mu_0 m}{4\pi})^2 \frac{1}{r^7}(\frac{5}{2}sin(2\theta)) - \frac{sin(2\theta)}{2}(\frac{\mu_0 m}{2\pi r^4} B_0 + \frac{1}{r} B_0^2)] \end{cases} \tag{32}$$

The expression of the magnetomotive force charts an elliptical motion and both terms have twice the excitation frequency. However, adding the homogeneous magnetic field decreases the force acting on the particle. Figure 37 shows the comparison between the standard magnetomotive technique and the addition of the coil running parallel and perpendicularly.

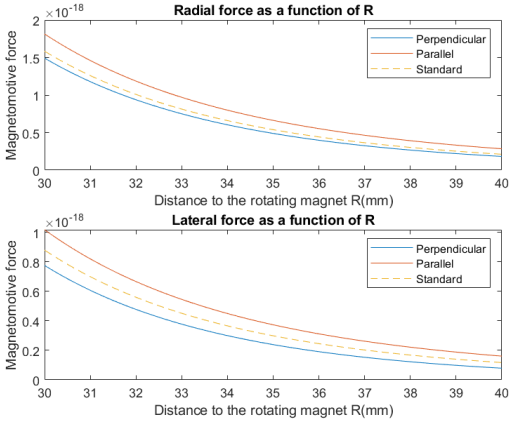

Figure 37: Magnetomotive force as a function of the distance between the magnetic probe and the particles for a 10mT homogeneous magnetic field.

The magnetic field generated by the Helmholtz coil was chosen in phase with the lateral components of the magnetic field produced by the magnetic probe. Introducing a phase difference between the magnetic fields could be investigated. From there, if there is an increase of the magnetomotive force in one direction, the position of the ultrasound probe could be adapted to detect the motion in the interesting direction.